Hilbert Space in Isotopologue Dy(III) SMM Dimers: Dipole Interaction Limit in $[^{163/164}Dy_2(tmhd)_6(tape)]^0$ Complexes

Ting-Ting Ruan, Eufemio Moreno-Pineda,* Michael Schulze, Sören Schlittenhardt, Thomas Brietzke, Hans-Jürgen Holdt, Senthil Kumar Kuppusamy, Wolfgang Wernsdorfer,* and Mario Ruben*

ABSTRACT: Single-molecule magnets are molecular complexes proposed to be useful for information storage and quantum information processing applications. In the quest for multilevel systems that can act as Qu*d*its, two dysprosium-based isotopologues were synthesized and characterized. The isotopologues are $[^{164}Dy_2(tmhd)_6(tape)]$ ($\mathbf{1}^{(I=0)}$) and $[^{163}Dy_2(tmhd)_6(tape)]$ ($\mathbf{2}^{(I=5/2)}$), where tmhd = 2,2,6,6-tetramethylheptandionate and tape = 1,6,7,12-tetraazaperylene. Both complexes showed slow relaxation at a zero applied magnetic field with dominant Orbach and Raman relaxation mechanisms. μSQUID studies at milli-Kelvin temperatures reveal quasi-single ion loops, in contrast with the expected S-shape (near zero field) butterfly loops, characteristic of antiferromagnetically coupled dimeric complexes. Through analysis of the low-temperature data, we find that the interaction operating between Dy(III) is small, leading to a small exchange biasing from the zero-field transition. The resulting indirectly coupled nuclear states are degenerate or possess a small energy difference between them. We, therefore, conclude that for the creation of Qu*d*its with enlarged Hilbert spaces, shorter Dy(III)···Dy(III) distances are deemed essential.

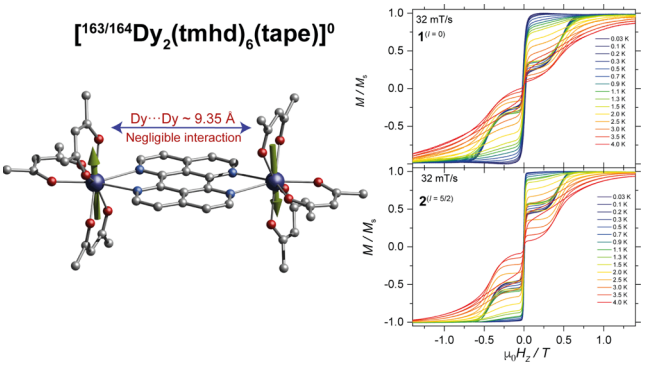

INTRODUCTION

Single-molecule magnets (SMMs) have been intensely investigated due to their possible implementation in quantum computing,[1−3] high-density information storage,[4−6] and spintronics.[7−9] Conversely to the 3d-SMM analogues, the SMM character of lanthanide-based complexes arises from the large intrinsic magnetic anisotropy of the lanthanide, resulting from the unquenched first-order orbital angular momentum of the shielded f-electrons, the strong spin−orbit coupling, and the ligand-field perturbation.[10−12] Lanthanide ions with significant intrinsic anisotropy and large ground-state spin, such as Dy(III), were shown to possess high energy barriers for relaxation of the magnetization, with blocking temperatures above liquid nitrogen.[13,14] Moreover, Ln-SMM systems were proposed as scaffolds for quantum information processing (QIP) schemes.[15−17] Such a proposal was validated by the execution of a quantum algorithm,[18] employing a single molecular unit of the archetypal $[TbPc_2]^0$ SMM embedded in a hybrid spintronic structure.[9,19−24]

At the molecular QIP level, the execution of the Grover algorithm, employing a single molecule of $[TbPc_2]^0$, was possible due to the four available nuclear states for computation, i.e., its multilevel character.[18] The exploitation of the nuclear states in $[TbPc_2]^0$ is a result of (i) the strong anisotropic character of the SMM, which isolates the electronic ground doublet state; (ii) the electronic state coupled to the nuclear spins embedded within the lanthanide through a strong hyperfine interaction. The hyperfine interaction splits the ground doublet state into $(2I + 1)$ states, where I is the nuclear spin of the lanthanide. (iii) Quantum tunneling of the magnetization[25] (QTM), occurring at some specific level crossings, allowing the initialization, manipulation, and read-out of the nuclear states.[2,18,22] Systems with more than two available states are coined as Qu*d*its, where d denotes the dimensionality.[2,26] Expectedly, SMMs with more available states, could in principle, allow the execution of more complex algorithms; hence, the synthesis of such systems is continuously explored.[26−31] Likewise, Qu*d*its have been predicted to reduce the number of iterations in quantum computation algorithms, diminish error rates, and allow error correction schemes.[2]

For the synthesis of Qu*d*its with a large Hilbert space, Dy(III) ions have been widely explored. The choice of the

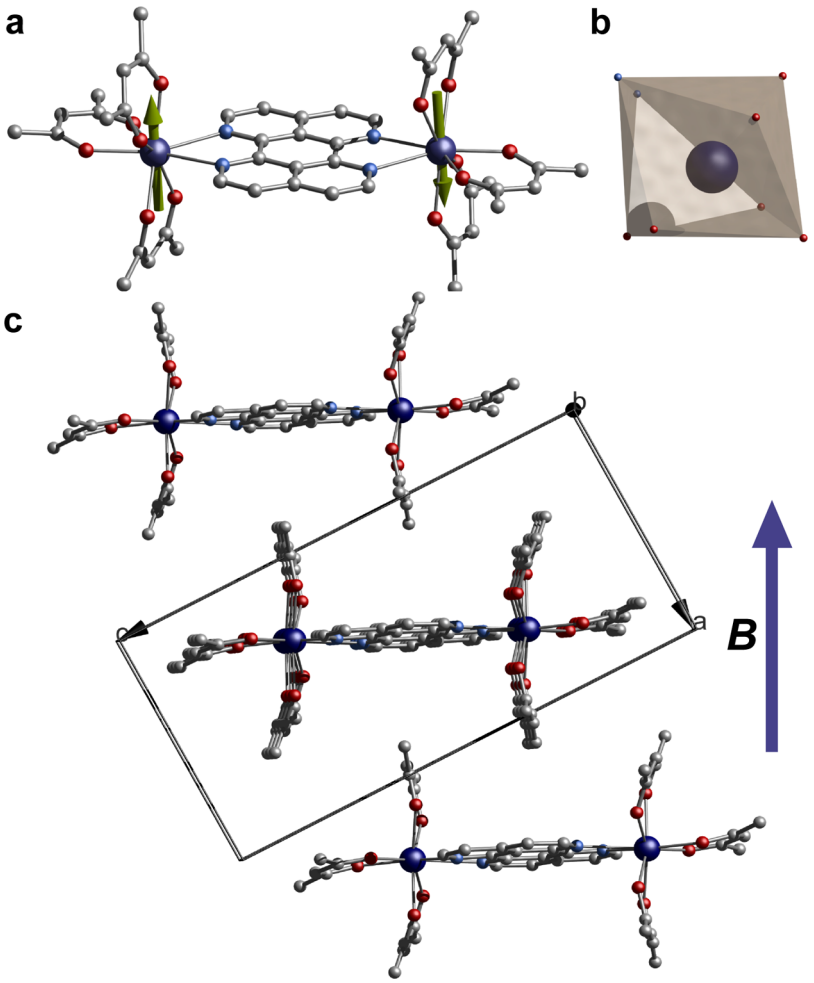

Figure 1. (a) Molecular structure of $[^{163}Dy_2(tmhd)_6(tape)]$ as obtained from single-crystal X-ray studies. The green arrows represent the anisotropy axis for each Dy(III) obtained from ab initio CASSCF calculations. (b) Polyhedral representation of the Dy(III) site on a N_2O_6 geometry. (c) Packing diagram of complex $[(Dy_2(tmhd)_6(tape)]$ parallel to the *ab* plane. The blue arrow denotes the applied field along the crystallographic axis for the μSQUID studies. Hydrogen and methyl groups have been omitted for clarity. Color code: C, gray; N, pale blue; O, red; Dy, dark blue.

Dy(III) ion is obvious since it has significant magnetic anisotropy and a large spin ground state, and as a Kramers ion, a doublet ground state is always rendered. Moreover, seven isotopes of Dy(III) are found in nature, with two different nuclear spin states, $I = 0$ for ^{160,162,164}Dy(III) and $I = 5/2$ for ^{161,163}Dy(III). Henceforth, SMMs incorporating ^{161,163}Dy(III) ($I = 5/2$) are appealing to increase the Hilbert space available for computation.[26−31] Clearly, the extension of the Hilbert space in mononuclear systems is limited by the nuclear spins; therefore, as an alternative, the indirect coupling of the nuclear states via an electronic interaction has been demonstrated.[32,33] The interaction (dipolar or exchange) between the electronic spins of a dimeric (or multimeric) complex can couple the nuclear states, leading to an exponential increment of the available states in the Qu*d*it, i.e., $(2I + 1)^n$. With these in mind, we synthesized two isotopically enriched dysprosium dinuclear SMMs, $[^{164}Dy_2(tmhd)_6(tape)]$ ($\mathbf{1}^{(I=0)}$) and $[^{163}Dy_2(tmhd)_6(tape)]$ ($\mathbf{2}^{(I=5/2)}$), with tmhd = 2,2,6,6-tetramethylheptandionate and tape = 1,6,7,12-tetraazaperylene. Complexes **1** and **2** are the first dinuclear lanthanide complexes containing tape, a highly π conjugated polyheteroaromatic molecule, as a bridging ligand. This rigid bis(α,α'-diimine) ligand combines an efficient metal−metal bridging capacity with a strong π accepting nature due to a low-lying π*MO. While the nuclear-spin-containing system can in principle act as a Qu*d*it, the nuclear-spin-free system allows the comprehension of the electronic characteristic of the complex, e.g., the interaction operating between the Dy(III) ions. The two complexes showed SMM characteristics in the absence of an applied magnetic field. AC-SQUID measurements, along with single-crystal μSQUID studies at sub-Kelvin temperatures, reveal a quasi-single-ion behavior. Although it has been shown that purely dipolar interaction permits the Hilbert space expansion in dinuclear SMMs,[27,33] we find that when the dipolar interaction is weak and the energies involved are rather small, it would make the utilization of the multilevel system as Qu*d*it more difficult. Consequently, for enlarged Hilbert spaces, shorter Dy(III)···Dy(III) atoms are deemed important.

RESULTS AND DISCUSSION

Syntheses and Structures. Complexes $\mathbf{1}^{(I=0)}$ and $\mathbf{2}^{(I=5/2)}$ were synthesized by reacting one equivalent of ligand tape with 2 equiv of $Ln(tmhd)_3(H_2O)_2$ precursor, in which Ln = ^{164}Dy(III) ($I = 0$) for $\mathbf{1}^{(I=0)}$ and ^{163}Dy(III) ($I = 5/2$) for $\mathbf{2}^{(I=5/2)}$, respectively (see the Supporting Information). The tape ligand was synthesized from 1,1′-bis-2,7-naphthyridine by

potassium-promoted cyclization in dimethoxyethane, followed by oxidation with air.[34] Homodinuclear ruthenium(II) complexes containing tape as a ligand can store one or two electrons in the energetically low-lying π^*-orbital,[35] while the diruthenium(II) complex of the disulfonato-substituted tape-$(SO_3)_2^{2-}$ was exploited as a redox mediator between an anaerobic homogeneous reaction solution of an enzyme system (sulfite/sulfite oxidase) and the electrode via participation of the low-energy π^*-orbital of the bridging ligand.[35] Crystals of $\mathbf{1}^{(I=0)}$ and $\mathbf{2}^{(I=5/2)}$, suitable for single-crystal X-ray studies, were grown from a mixture of ethanol and dichloromethane. X-ray studies reveal both complexes to be isomorphic, crystallizing in the triclinic $P\bar{1}$ space group. The molecular structures of both complexes are composed of two Dy(III) ions, six tmhd, and one bridging tape ligand (Figure 1a). The unit cell is occupied by a single molecule, with half molecule residing in the asymmetric unit. In both structures, the tape ligand coordinates to two Dy(III), with both dysprosium ions being equivalent through an inversion center.

In the crystal structure, the Dy(III) ions are surrounded by three tmhd ligands, each in a bidentate chelating fashion, while two nitrogens from the tape ligand form a N_2O_6 coordination geometry. The Dy−O distances are in the ranges 2.262(7)−2.356(8) Å for $\mathbf{1}^{(I=0)}$ and 2.251(1)−2.350(8) Å for $\mathbf{2}^{(I=5/2)}$, while the Dy−N distances range between 2.618(7)−2.657(8) Å for $\mathbf{1}^{(I=0)}$ and 2.617(7)−2.662(8) Å for $\mathbf{2}^{(I=5/2)}$. The intramolecular Dy···Dy distances are 9.3276(5) and 9.3326(5) Å for $\mathbf{1}^{(I=0)}$ and $\mathbf{2}^{(I=5/2)}$, respectively. The local coordination symmetries of the Dy(III) ions are best described as having triangular dodecahedron geometry (TDD-8) with deviation values of 0.615 and 0.603 for $\mathbf{1}^{(I=0)}$ and $\mathbf{2}^{(I=5/2)}$, respectively (Table S2).[37] The shortest intermolecular Dy···Dy distances are 9.8851(5) and 9.8745(5) Å for $\mathbf{1}^{(I=0)}$ and $\mathbf{2}^{(I=5/2)}$, respectively.

The phase purities of the polycrystalline samples of $\mathbf{1}^{(I=0)}$ and $\mathbf{2}^{(I=5/2)}$ were determined by powder X-ray diffraction (PXRD) analysis. The experimental PXRD patterns of $\mathbf{1}^{(I=0)}$ and $\mathbf{2}^{(I=5/2)}$ were all in excellent agreement with the simulated patterns (Figure S1), indicating that both samples are monophasic crystalline materials.

Magnetic Properties. *Static Magnetic Studies.* The static magnetic properties for $\mathbf{1}^{(I=0)}$ and $\mathbf{2}^{(I=5/2)}$ were studied employing polycrystalline samples in the temperature range of 2−300 K under an applied field of 1 kOe. Both $\chi_M T(T)$ profiles are very similar, with room temperature $\chi_M T(T)$ values of 28.00 and 28.14 $cm^3\ K\ mol^{-1}$ for $\mathbf{1}^{(I=0)}$ and $\mathbf{2}^{(I=5/2)}$, respectively (Figure 2). The values are comparable with the expected value of 28.34 $cm^3\ K\ mol^{-1}$ for two isolated Dy(III) with $J = 15/2$ and $g_J = 4/3$. Upon cooling, the $\chi_M T(T)$ values start gradually decreasing down to 5 K, where they rapidly drop to a minimum value of 18.4 $cm^3\ K\ mol^{-1}$ and 21.5 $cm^3\ K\ mol^{-1}$ (at 2 K) for $\mathbf{1}^{(I=0)}$ and $\mathbf{2}^{(I=5/2)}$, respectively. A sharp decrease of $\chi_M T$ upon cooling could be attributed to the depopulation of crystal field levels, antiferromagnetic interactions, and/or magnetic blocking (vide infra).

The $M(H)$ was likewise collected at 2, 3, 4, and 5 K, revealing a rapid increase at low magnetic fields (insets in Figure 2). At high magnetic fields, the saturation of magnetization was observed with values of 9.26 μ_B for $\mathbf{1}^{(I=0)}$ and 9.86 μ_B for $\mathbf{2}^{(I=5/2)}$, both at 7 T. The $M(H)$ values are in good agreement with expected values for two Dy(III) ions with well-defined $J = 15/2$ ground doublet, i.e., ∼10 μ_B, characteristic of anisotropic Dy(III) SMMs.

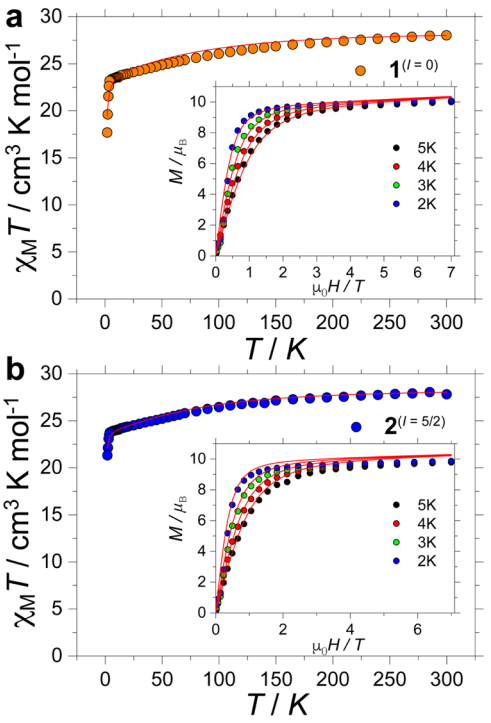

Figure 2. $\chi_M T(T)$ profiles for (a) $\mathbf{1}^{(I=0)}$ and (b) $\mathbf{2}^{(I=5/2)}$ and $M(H)$ at different temperatures (insets). Solid lines represent the fitting from ab initio calculations and the Lines model, as described in the text.

Dynamic Magnetic Properties. Although the static magnetic properties show the expected $\chi_M T(T)$ value for the dimeric Dy(III) complexes, it provides no conclusive signature of the magnetic anisotropy of the isotopologues. To probe the slow relaxation characteristics of $\mathbf{1}^{(I=0)}$ and $\mathbf{2}^{(I=5/2)}$, temperature- and frequency-dependent (in-phase (χ') and out-of-phase (χ'')) dynamic magnetic measurements were performed (Figures 3 and S2−S5). Dynamic measurements, under a zero applied dc field, reveal a maximum in the $\chi''(T; \nu)$ and a clear frequency-dependent signal below 20 K for both complexes, signaling SMM behavior (see Figures S3 and S5). Conversely, the frequency dependence of the susceptibility shows a clear difference between the two isotopologues (cf. Figure 3a,b). At the lowest measured temperature of 2 K, complex $\mathbf{1}^{(I=0)}$ shows a maximum centered at ca. 10 Hz, which stays practically constant up to reaching 6 K. In contrast, the maximum for $\mathbf{2}^{(I=5/2)}$ is centered at around 50 Hz at 2 K and stays close to this value until 6 K. Above 6 K, the maximum for both complexes shifts to higher frequencies upon increasing temperature up to 20 K (Figure 3a,b). The ac data of $\mathbf{1}^{(I=0)}$ and $\mathbf{2}^{(I=5/2)}$ can be fitted to a generalized Debye model. The Cole−Cole plots are close to semicircles (Figures S2 and S4), as expected. The relaxation time parameter α is found to be in the ranges 0.006(3)−0.17(1) for $\mathbf{1}^{(I=0)}$ and 0.16(3)−0.24(5) for $\mathbf{2}^{(I=5/2)}$. As observed, α highlights a narrower distribution of relaxations at lower temperatures for $\mathbf{1}^{(I=0)}$ compared to $\mathbf{2}^{(I=5/2)}$, while at higher temperatures, α is very similar. The similar behavior for $\mathbf{1}^{(I=0)}$ and $\mathbf{2}^{(I=5/2)}$ at high temperatures and the dissimilarities at low temperatures are consonant with the observed behavior in reported isotopologues, as nuclear spins play a major role at lower temperatures.[27]

The extracted $\tau(T)$ data from the Debye model for complexes $\mathbf{1}^{(I=0)}$ and $\mathbf{2}^{(I=5/2)}$ are depicted in Figure 3c,d. To

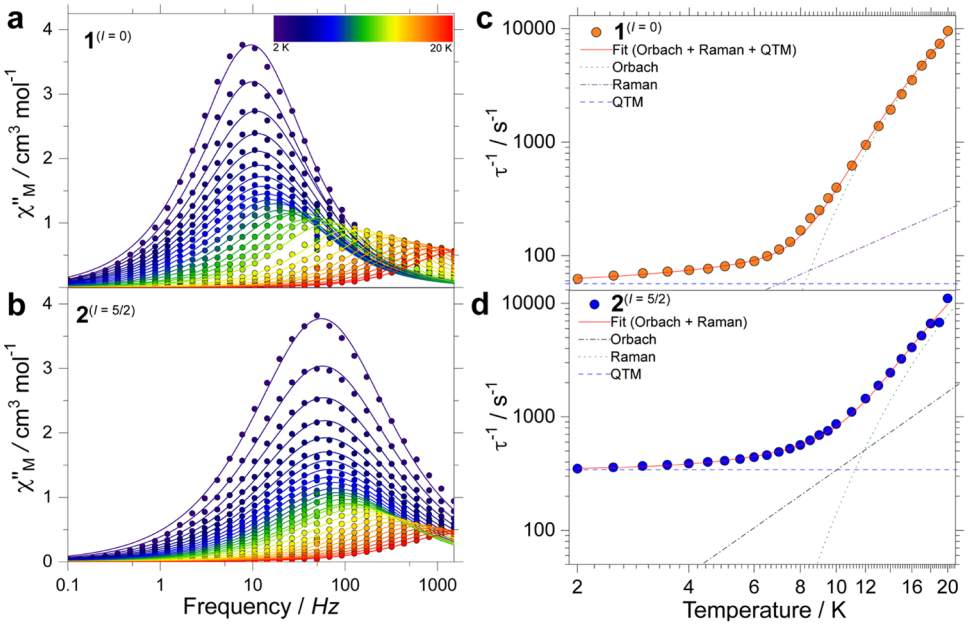

Figure 3. Experimental frequency-dependent magnetic susceptibility data at a zero applied DC (H_{DC}) field and variable temperatures ($\chi_M''(\nu)$) for (a) $\mathbf{1}^{(I=0)}$ and (b) $\mathbf{2}^{(I=5/2)}$. Panels (c) and (d) show the $\tau^{-1}(T)$ for $\mathbf{1}^{(I=0)}$ (a) and $\mathbf{2}^{(I=5/2)}$ (b). The solid red line in panels (c) and (d) is the best fit employing eq 1, whereas the green and the black dashed lines are the Orbach relaxation, Raman relaxation, and QTM contribution to the whole fit.

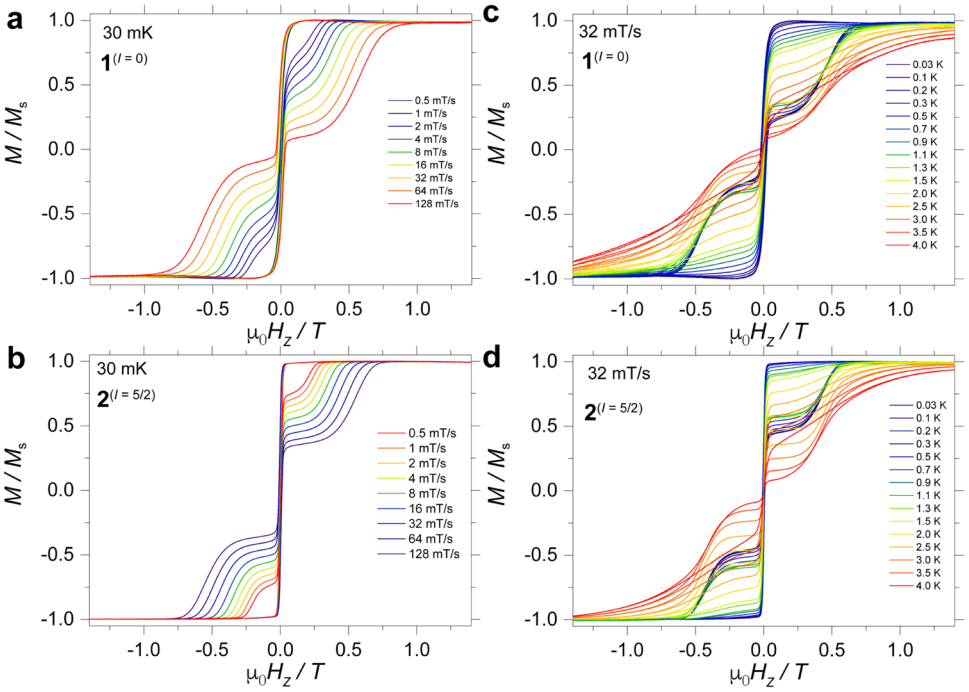

Figure 4. Sweep-rate-dependent μSQUID studies for (a) $\mathbf{1}^{(I=0)}$ and (b) $\mathbf{2}^{(I=5/2)}$ collected at 30 mK and temperature dependence of the μSQUID data for (c) $\mathbf{1}^{(I=0)}$ and (d) $\mathbf{2}^{(I=5/2)}$ collected at a sweep rate of 32 mT/s.

investigate the mechanisms inducing magnetization relaxation, the $\tau(T)$ was fitted to

$$\tau^{-1} = \tau_0^{-1}\exp(-U_{eff}/k_BT) + CT^n + \tau_{QTM}^{-1} \quad (1)$$

where the first term represents the Orbach process, the second one represents the Raman (CT^n) relaxation and the third term is the quantum tunneling of the magnetization (QTM) process. The best fitting affords an U_{eff} of 70(1) K (48.6 cm^{-1}), $\tau_0 = 3.5(3) \times 10^{-6}$ s, $C = 2.4(2)$ s^{-1} K^{-n}, $n = 1.4(3)$, and $\tau_{QTM} = 0.018(1)$ s for $\mathbf{1}^{(I=0)}$, and U_{eff} of 80(4) K (55.6 cm^{-1}), $\tau_0 = 2.3(5) \times 10^{-6}$ s, $C = 1.7(8)$ s^{-1} K^{-n}, $n = 2.3(2)$ and $\tau_{QTM} = 0.029(3)$ s for $\mathbf{2}^{(I=5/2)}$. As expected, both barriers are similar, while the value of C shows some differences in the Raman process, suggesting that the Raman relaxation process is readily enhanced by the presence of the nuclear spin in $\mathbf{2}^{(I=5/2)}$.[27] Note that the Raman n parameter is lower than that expected for a purely Kramers ion, implying that acoustic and/or optic phonons are active.[25,36]

Low-Temperature μ-SQUID Studies. To investigate the Qudit characteristic of the isotopologues, we turned our

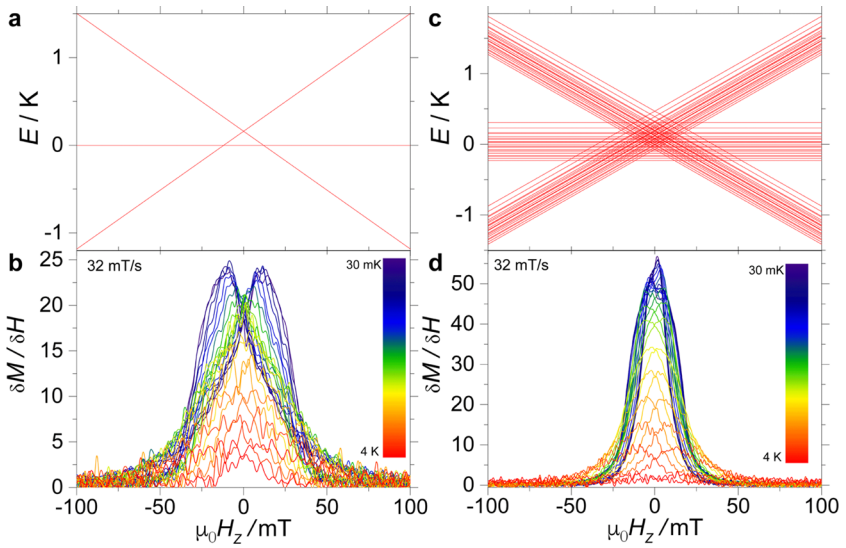

Figure 5. Zeeman diagram obtained employing eqs 3 and 4 for (a) $\mathbf{1}^{(I=0)}$ and (c) $\mathbf{2}^{(I=5/2)}$, respectively. Derivative of the temperature-dependent hysteresis loops from μSQUID studies for (b) $\mathbf{1}^{(I=0)}$ and (d) $\mathbf{2}^{(I=5/2)}$.

attention to μSQUID studies at sub-Kelvin temperatures. μSQUID allows us to probe the differences in the relaxation dynamics and nuclear spin effects. Furthermore, μ-SQUID investigations permit the investigation of hyperfine-driven QTM[25,37] (*hf*-QTM) and exchange-bias QTM,[38−42] important characteristics for the exploitation of SMMs in quantum computing applications. The studies were carried out on single crystals of $\mathbf{1}^{(I=0)}$ and $\mathbf{2}^{(I=5/2)}$ with the field applied along the easy axis of the crystal.[43,44] Hysteresis loop studies were performed at different sweeping rates ranging from 0.5 to 128 mT/s and temperatures from 4 to 30 mK (Figure 4).

A large step at zero field is observed for both complexes in the sweeping rate dependence and the temperature dependence of the loops. While this is expected for single-ion magnets (SIMs), due to the fast relaxation, typically QTM, the lack of S-shape hysteresis loops near zero field, characteristic of antiferromagnetically coupled dimeric SMMs, highlights a negligible dipolar/exchange interaction between the Dy(III) centers. As shown in Figure 4, the hysteresis loops become narrow with increasing temperatures and decreasing sweep rates, confirming the SMM behavior of $\mathbf{1}^{(I=0)}$ and $\mathbf{2}^{(I=5/2)}$. Above $\mu_0 H_Z = \pm 0.25$ T, the loops have a broad step, which is strongly dependent on the field-sweep rate and is a consequence of the direct relaxation process. Note that wider loops are observed for $\mathbf{1}^{(I=0)}$ compared to $\mathbf{2}^{(I=5/2)}$ due to the lack of nuclear spins. It should be noticed that the loops for $\mathbf{2}^{(I=5/2)}$ show a more sweep-dependent behavior than those for $\mathbf{1}^{(I=0)}$, denoting that the nuclear spins can enhance relaxation by facilitating the coupling to the phonon bath.[27]

Theoretical Calculations. To comprehend the static, dynamic, and μSQUID data, CASSCF calculations were performed for $\mathbf{1}^{(I=0)}$ and $\mathbf{2}^{(I=5/2)}$. The calculations were carried out on monometallic Dy(III) fragments (Figure S6) of $\mathbf{1}^{(I=0)}$ and $\mathbf{2}^{(I=5/2)}$, employing MOLCAS 8.2 (see the Supporting Information). Expectedly, based on crystallographic and geometrical considerations, the characteristics of both complexes are very similar. The effective g_z tensors for $\mathbf{1}^{(I=0)}$ and $\mathbf{2}^{(I=5/2)}$ of 19.4918 and 19.4268, respectively, are close to the Ising-limit value of 20, characteristic of significant uniaxial anisotropy. The m_J components for the eight lowest Kramer doublets (KDs) of each Dy(III) ion for complexes $\mathbf{1}^{(I=0)}$ and $\mathbf{2}^{(I=5/2)}$ are shown in Tables S5 and S6, respectively. The ground KDs for Dy(III) fragments are all predominantly composed of $m_J = \pm 15/2$, and their first excited states are mostly composed of a mixture of several m_J states (Tables S5 and S6). The energy barrier of the thermally excited Orbach process relates to the energy gap between the ground state and first excited state. The obtained energy gaps between the ground and the first excited KDs for the Dy(III) fragments of $\mathbf{1}^{(I=0)}$ and $\mathbf{2}^{(I=5/2)}$ are 251.2 K (174.6 cm^{-1}) and 236.9 K (164.7 cm^{-1}), respectively, which are much greater than obtained via dynamic studies, i.e., U_{eff} = 67.5 K (46.9 cm^{-1}) ($\mathbf{1}^{(I=0)}$) and 66.3 K (46.1 cm^{-1}) ($\mathbf{2}^{(I=5/2)}$). These deviations are probably due to the coexistence of multiple relaxation processes.[45] Inspection of the calculated transverse magnetic moments, acting as a proxy for the relaxation, shows that relaxation through excited states is the most efficient pathway.

Up to this point, the discussion is based on the isolated Dy(III) ion; however, interactions between Dy(III) atoms can play a significant role in the relaxation dynamics. To evaluate the interaction operating between the Dy(III) ions, the Lines model[46] was employed to fit the magnetic susceptibilities of complexes $\mathbf{1}^{(I=0)}$ and $\mathbf{2}^{(I=5/2)}$. The Lines model uses an isotropic exchange between the spin component of the angular momenta (S = 5/2 for Dy(III)) and the crystal field parameters obtained via the CASSCF calculations.[47,48] The Hamiltonian has the form

$$\mathcal{H}^{i}_{Dy} = \mathcal{H}^{i}_{lf} + g_J \mu_0 \mu_B (\hat{J}_{Dy(1)} + \hat{J}_{Dy(2)}) \mathbf{H_z} + \boldsymbol{J}^{i}_{\mathbf{Lines}} (\hat{S}_{Dy(1)} + \hat{S}_{Dy(2)}) \quad (2)$$

where $\mathcal{H}^{i}_{lf} = \sum_{k=2,4,6,-k\le q\le k} u_k B^q_k O^q_k$ is the ligand-field Hamiltonian expressed in the Steven's operator, u_i are the Stevens factors, O^q_k are the Stevens operator, and B^q_k are the ligand field parameters obtained from CASSCF calculations. $\hat{J}_{Dy(i)}$ and $_{Dy(i)}$ are the spin−orbit and spin-only states for Dy(III), respectively. Simultaneous fitting[49] of $\chi_M T(T)$ and $M(H)$, employing the crystal field parameters as determined from CASSCF, yields a J_{Lines} = 19(1) mK (0.013(1) cm^{-1}) for $\mathbf{1}^{(I=0)}$ and 1.4(3) mK (0.97(3) × 10^{-3} cm^{-1}) for $\mathbf{2}^{(I=5/2)}$ (see Figure 2). Simulation of $\chi_M T(T)$ and $M(H)$ without the inclusion of

an interaction operating between the Dy(III) centers does reproduce most of the profile, except for the low-temperature (<5 K) downturn in $\chi_M T(T)$.

It is important to note that at first glance, an absence of S-shape near zero-field loops highlights negligible or nonexistent interactions operating between the Dy(III) centers. Nonetheless, careful examination of the derivative of the temperature-dependent hysteresis loops (Figure 5b) reveals a tunneling event occurring at ±12 mT in $\mathbf{1}^{(I=0)}$, while for $\mathbf{2}^{(I=5/2)}$, tunneling is spread out over a ±50 mT range. For $\mathbf{1}^{(I=0)}$, the tunneling event at ±12 mT allows the direct estimation of the exchange coupling J_{ex} between the two Dy(III) ions through $H_{ex} = J_{ex} m_J / g_J \mu_\beta$, where $m_J = 15/2$, $g_J = 4/3$, and μ_β is the Bohr magneton. J_{ex} is found to be 1.43 mK (9.91×10^{-4} cm^{-1}) for $\mathbf{1}^{(I=0)}$. The determined J_{ex} is in good agreement with the one estimated from a purely point dipolar approximation: J_{zz}^{dip} = 1.36 mK (9.45×10^{-4} cm^{-1}) for a ^{164}Dy···^{164}Dy distance of 9.3326(5) Å; hence, the interaction between the Dy(III) pairs is purely of dipolar origin. Note that a direct comparison between J_{ex} and J_{Lines} is not possible. The small antiferromagnetic interaction observed in the μSQUID loops is consistent with the observed crossing in the μSQUID loops (vide infra).

To better comprehend the μSQUID results, we modeled the low-temperature magnetic properties of $\mathbf{1}^{(I=0)}$ and $\mathbf{2}^{(I=5/2)}$. First, for simplicity, we solely consider $\mathbf{1}^{(I=0)}$. The single-ion magnetic properties of the SMM are dominated by the spin–orbit coupling and the interaction with the surrounding ligands, leading to a large separation between the ground m_J = ±15/2 and the first excited m_J = ±13/2 multiplet. This allows us to describe the complex as two isolated Ising spins ($s = 1/2$) coupled through an effective interaction $J_{ex}\sigma_{1z}\,\sigma_{2z}$, where J_{ex} is an effective coupling and $\sigma_{1z,2z}$ are the z-Pauli matrices. Thus, under the action of an external magnetic field applied along the easy axis, the Hamiltonian for $\mathbf{1}^{(I=0)}$ is written as

$$^{164}\mathcal{H} = g_{eff}\mu_B\mu_0 H_z(\sigma_{1z} + \sigma_{2z}) + J_{ex}\sigma_{1z}\sigma_{2z} \quad (3)$$

where g_{eff} = 20 and J_{ex} is the interaction between the ions (projected on $s = 1/2$ basis). For $\mathbf{2}^{(I=5/2)}$, the complex bearing a nuclear spin, the Hamiltonian incorporates the hyperfine (A_{hyp}) and quadrupolar (P_{quad}) interactions

$$^{163}\mathcal{H} = ^{164}\mathcal{H} + \sum_{i=1}^{2} A_{hyp}\mathbf{I}^i\cdot\boldsymbol{\sigma}_i + P_{quad}I_z^i I_z^i \quad (4)$$

The Zeeman diagram for $\mathbf{1}^{(I=0)}$ is shown in Figure 5a. In the case of $\mathbf{2}^{(I=5/2)}$, the Zeeman diagram was obtained by fixing J_{ex} to the one obtained for $\mathbf{1}^{(I=0)}$, while the hyperfine and quadrupolar interactions were fixed to A_{hyp} = 107.1 mK (0.074 cm^{-1}) and P_{quad} = 19.6 mK (0.014 cm^{-1})[27] (Figure 5c). As observed, for $\mathbf{1}^{(I=0)}$, QTM is possible at the crossings between the ground singlet and the excited doublet (±12 mT) due to the lack of nuclear spins states. Conversely, $\mathbf{2}^{(I=5/2)}$ contains a nuclear spin, which can induce *hf*-QTM, shifting the QTM event from zero to certain field values. However, the interaction between the Dy(III) centers can induce the indirect coupling of the nuclear states, hence creating $(2I + 1)^n$ states, with a multitude of crossing, where *hf*-QTM is active and the system can relax. Also, note that the shortest intermolecular Dy···Dy is 0.5 Å longer than the intramolecular interaction. This, along with the μSQUID results, indicates that the intramolecular interaction is mainly responsible for the coupled behavior.

This is clearly visible in the width of the loops (Figure 4), being narrower in $\mathbf{1}^{(I=0)}$ compared with $\mathbf{2}^{(I=5/2)}$. In the derivative loops (Figure 5b,d), it can be observed that for $\mathbf{1}^{(I=0)}$, QTM is more efficient at ±12 mT. In an ideal scenario, for $\mathbf{1}^{(I=0)}$, QTM would only be expected at ±12 mT, with no QTM anywhere in the field range. Nonetheless, the polycrystalline and non-diluted nature of the sample is responsible for the broadening of the ideal transitions. In contrast, for $\mathbf{2}^{(I=5/2)}$, tunneling occurs between ±50 mT, with strong QTM occurring between ±20 mT. This is a result of the multitude of nuclear-spin-coupled states, many of them at which QTM is active. The effect of the nuclear states is to broaden QTM relaxation through the ±50 mT field range. Note that while the interaction between the lanthanides is important for the synthesis of Qu*d*its, the interaction found in this study is small, causing a small shift from the zero-field transition.

The successful execution of the Groover's algorithm employing the hyperfine states embedded in a single $TbPc_2$ molecule was possible due to the sizable difference between the hyperfine states of the molecule.[18,23] This difference allows the selective initialization, manipulation, and read-out of the nuclear states of the system. Similarly, we have reported the hyperfine-coupled nuclear-stated read-out in a Tb_2Pc_3 unit,[32] steaming from the hyperfine interaction and electronic interaction between the Tb(III) units. In this case, although a total of 16 hyperfine states arise from the electronic interaction, only seven would be suitable for nuclear spin manipulation, given that the remaining states are degenerate.[32,33] These observations allow us to conclude that for successful exploitation of the nuclear-spin-coupled states in Qu*d*its, a sizable electronic interaction is required with considerable separation between the hyperfine-coupled states. In contrast, we find that the hyperfine-coupled states in $\mathbf{2}^{(I=5/2)}$ have a minute energy difference and in many cases are degenerate. The small difference between the hyperfine states might require further efforts for the operation of many hyperfine-coupled states. Another plausible alternative to increase the energy difference between the hyperfine-coupled states would be to increment the hyperfine interaction, which could be achievable by reducing the trivalent lanthanide to a divalent analogue.[50−53] Certainly, divalent lanthanide (Ln) complexes, with an unusual electronic configuration of Ln(II), exhibit a strong interaction between the nuclear spin and the electronic degrees of freedom, allowing for the electrical tuning of the interaction. As an example, in a neutral $Tb(II)(CpiPr_5)_2$ single-molecule magnet (SMM), the hyperfine interaction of the ^{159}Tb nucleus is approximately 1 order of magnitude greater than that observed in $Tb(III)Pc_2$ SMMs.[54] Moreover, the hyperfine constant of ^{163}Dy(II) is measured to be 162.6 MHz, which is greater than that of ^{163}Dy(III), recorded as 152.4 MHz.[55−57] Consequently, reducing ^{163}Dy(III) to ^{163}Dy-(II) has the potential to further increase the level of the hyperfine interaction.

CONCLUSIONS

Two dinuclear $^{163/164}$Dy isotopologues have been successfully synthesized, and their structures and magnetic properties have been characterized. Through ac studies, we find that the presence of the nuclear spin plays an important role at low temperatures in the relaxation mechanism, as observed in the Raman dependence, while the high-temperature data is insensitive to the nuclear spins. Sub-Kelvin μSQUID studies

likewise reveal fast relaxation near zero-field for both complexes, with slightly larger open loops for $\mathbf{1}^{(I=0)}$. The large step at zero field in the loops observed for both complexes is typical for single-ion lanthanide-based SMMs, indicating that there is no or only a negligible interaction operating between the two Dy(III) ions. Judicious analysis of the μSQUID loops reveals a small interaction operating between the Dy(III) ions, which is expected for an interaction purely of dipolar origin but can be considered as responsible for a weak coupling of the nuclear spins in $\mathbf{2}^{(I=5/2)}$. In contrast to our previous report, where we investigated the relaxation dynamics of two isotopologues in different temperature range,[27] herein, we show that the strength of the intramolecular interaction (of exchange or dipolar origin) is important to span the Hilbert space of Qudits; hence, shorter Dy(III)···Dy(III) are desired.

AUTHOR INFORMATION

Corresponding Authors

Eufemio Moreno-Pineda − *Depto. de Química-Física, Facultad de Ciencias Naturales, Exactas y Tecnología, Universidad de Panamá, Panamá 0824, Panamá; Grupo de Investigación de Materiales, Facultad de Ciencias Naturales, Exactas y Tecnología, Universidad de Panamá, Panamá 0824, Panamá;* orcid.org/0000-0002-9643-0341; Email: eufemio.moreno@up.ac.pa

Wolfgang Wernsdorfer − *Physikalisches Institut, Karlsruhe Institute of Technology, D-76131 Karlsruhe, Germany;* orcid.org/0000-0003-4602-5257; Email: wolfgang.wernsdorfer@kit.edu

Mario Ruben − *Institute of Nanotechnology (INT), Karlsruhe Institute of Technology (KIT), D-76344 Eggenstein-Leopoldshafen, Germany; Institute of Quantum Materials and Technologies (IQMT), Karlsruhe Institute of Technology (KIT), 76344 Eggenstein-Leopoldshafen, Germany; Centre Européen de Sciences Quantiques (CESQ), Institut de Science et d'Ingénierie Supramoléculaires (ISIS), 67083 Strasbourg, France*; Email: mario.ruben@kit.edu

Authors

Ting-Ting Ruan − *Institute of Nanotechnology (INT), Karlsruhe Institute of Technology (KIT), D-76344 Eggenstein-Leopoldshafen, Germany*

Michael Schulze − *Physikalisches Institut, Karlsruhe Institute of Technology, D-76131 Karlsruhe, Germany;* orcid.org/0000-0002-7169-0630

Sören Schlittenhardt − *Institute of Nanotechnology (INT), Karlsruhe Institute of Technology (KIT), D-76344 Eggenstein-Leopoldshafen, Germany*

Thomas Brietzke − *Anorganische Chemie, Institut für Chemie, Universität Potsdam, D-14476 Potsdam, Germany*

Hans-Jürgen Holdt − *Anorganische Chemie, Institut für Chemie, Universität Potsdam, D-14476 Potsdam, Germany;* orcid.org/0000-0002-8121-6254

Senthil Kumar Kuppusamy − *Institute of Quantum Materials and Technologies (IQMT), Karlsruhe Institute of Technology (KIT), 76344 Eggenstein-Leopoldshafen, Germany;* orcid.org/0000-0002-1501-7759

Notes

The authors declare no competing financial interest.

ACKNOWLEDGMENTS

The authors acknowledge the DFG-CCR 1573 "4f for future" (project B3) and the Karlsruhe Nano Micro Facility (KNMF, www.kit.edu/knmf) for the provision of access to instruments at their laboratories. T.-T.R. acknowledges the China Scholarship Council (No. 201806650008). E.M.-P. thanks to the Panamanian National System of Investigators (SNI, SENACYT) and SENACYT (project PFID-FID-2021-60) for support. W.W. thanks the A.v. Humboldt foundation and the ERC grant MoQuOS No. 741276.

REFERENCES

(1) Moreno-Pineda, E.; Wernsdorfer, W. Measuring Molecular Magnets for Quantum Technologies. *Nat. Rev. Phys.* **2021**, *3* (9), 645−659.

(2) Moreno-Pineda, E.; Godfrin, C.; Balestro, F.; Wernsdorfer, W.; Ruben, M. Molecular Spin Qudits for Quantum Algorithms. *Chem. Soc. Rev.* **2018**, *47* (2), 501−513.

(3) Leuenberger, M. N.; Loss, D. Quantum Computing in Molecular Magnets. *Nature* **2001**, *410* (6830), 789−793.

(4) Gatteschi, D.; Sessoli, R.; Villain, J.*Molecular Nanomagnets*; Oxford University Press: USA, 2006; Vol. *5*.

(5) Liddle, S. T.; van Slageren, J. Improving F-Element Single Molecule Magnets. *Chem. Soc. Rev.* **2015**, *44* (19), 6655−6669.

(6) Woodruff, D. N.; Winpenny, R. E. P.; Layfield, R. A. Lanthanide Single-Molecule Magnets. *Chem. Rev.* **2013**, *113* (7), 5110−5148.

(7) Bogani, L.; Wernsdorfer, W. Molecular Spintronics Using Single-Molecule Magnets. *Nat. Mater.* **2008**, *7* (3), 179−186.

(8) Candini, A.; Klyatskaya, S.; Ruben, M.; Wernsdorfer, W.; Affronte, M. Graphene Spintronic Devices with Molecular Nanomagnets. *Nano Lett.* **2011**, *11* (7), 2634−2639.

(9) Vincent, R.; Klyatskaya, S.; Ruben, M.; Wernsdorfer, W.; Balestro, F. Electronic Read-out of a Single Nuclear Spin Using a Molecular Spin Transistor. *Nature* **2012**, *488* (7411), 357−360.

(10) Zhang, P.; Guo, Y. N.; Tang, J. Recent Advances in Dysprosium-Based Single Molecule Magnets: Structural Overview and Synthetic Strategies. *Coord. Chem. Rev.* **2013**, *257* (11−12), 1728−1763.

(11) Gatteschi, D. Anisotropic Dysprosium. *Nat. Chem.* **2011**, *3* (10), No. 830.

(12) Habib, F.; Murugesu, M. Lessons Learned from Dinuclear Lanthanide Nano-Magnets. *Chem. Soc. Rev.* **2013**, *42* (8), 3278−3288.

(13) Gould, C. A.; McClain, K. R.; Reta, D.; Kragskow, J. G. C.; Marchiori, D. A.; Lachman, E.; Choi, E.; Analytis, J. G.; Britt, R. D.; Chilton, N. F.; Harvey, B. G.; Long, J. R. Ultrahard Magnetism from Mixed-Valence Dilanthanide Complexes with Metal-Metal Bonding. *Science* **2022**, *375* (6577), 198−202.

(14) Guo, F. S.; Day, B. M.; Chen, Y. C.; Tong, M. L.; Mansikkamäki, A.; Layfield, R. A. Magnetic Hysteresis up to 80 K in a Dysprosium Metallocene Single-Molecule Magnet. *Science* **2018**, *362* (6421), 1400−1403.
(15) Troiani, F.; Affronte, M. Molecular Spins for Quantum Information Technologies. *Chem. Soc. Rev.* **2011**, *40* (6), 3119−3129.
(16) Gaita-Ariño, A.; Luis, F.; Hill, S.; Coronado, E. Molecular Spins for Quantum Computation. *Nat. Chem.* **2019**, *11* (4), 301−309.
(17) Lehmann, J.; Gaita-Ariño, A.; Coronado, E.; Loss, D. Quantum Computing with Molecular Spin Systems. *J. Mater. Chem.* **2009**, *19* (12), 1672−1677.
(18) Godfrin, C.; Ferhat, A.; Ballou, R.; Klyatskaya, S.; Ruben, M.; Wernsdorfer, W.; Balestro, F. Operating Quantum States in Single Magnetic Molecules: Implementation of Grover's Quantum Algorithm. *Phys. Rev. Lett.* **2017**, *119* (18), No. 187702.
(19) Godfrin, C.; Thiele, S.; Ferhat, A.; Klyatskaya, S.; Ruben, M.; Wernsdorfer, W.; Balestro, F. Electrical Read-Out of a Single Spin Using an Exchange-Coupled Quantum Dot. *ACS Nano* **2017**, *11* (4), 3984−3989.
(20) Troiani, F.; Godfrin, C.; Thiele, S.; Balestro, F.; Wernsdorfer, W.; Klyatskaya, S.; Ruben, M.; Affronte, M. Landau-Zener Transition in a Continuously Measured Single-Molecule Spin Transistor. *Phys. Rev. Lett.* **2017**, *118* (25), No. 257701.
(21) Godfrin, C.; Lumetti, S.; Biard, H.; Bonet, E.; Klyatskaya, S.; Ruben, M.; Candini, A.; Affronte, M.; Wernsdorfer, W.; Balestro, F. Microwave-Assisted Reversal of a Single Electron Spin. *J. Appl. Phys.* **2019**, *125* (14), No. 142801.
(22) Godfrin, C.; Ballou, R.; Bonet, E.; Ruben, M.; Klyatskaya, S.; Wernsdorfer, W.; Balestro, F. Generalized Ramsey Interferometry Explored with a Single Nuclear Spin Qudit. *npj Quantum Inf.* **2018**, *4* (1), No. 53.
(23) Thiele, S.; Balestro, F.; Ballou, R.; Klyatskaya, S.; Ruben, M.; Wernsdorfer, W. Electrically Driven Nuclear Spin Resonance in Single-Molecule Magnets. *Science* **2014**, *344* (6188), 1135−1138.
(24) Thiele, S.; Vincent, R.; Holzmann, M.; Klyatskaya, S.; Ruben, M.; Balestro, F.; Wernsdorfer, W. Electrical Readout of Individual Nuclear Spin Trajectories in a Single-Molecule Magnet Spin Transistor. *Phys. Rev. Lett.* **2013**, *111* (3), No. 037203.
(25) Ishikawa, N.; Sugita, M.; Wernsdorfer, W. Quantum Tunneling of Magnetization in Lanthanide Single-Molecule Magnets: Bis(Phthalocyaninato)Terbium and Bis(Phthalocyaninato)Dysprosium Anions. *Angew. Chem., Int. Ed.* **2005**, *44* (19), 2931−2935.
(26) Wernsdorfer, W.; Ruben, M. Synthetic Hilbert Space Engineering of Molecular Qudits: Isotopologue Chemistry. *Adv. Mater.* **2019**, *31* (26), No. 1806687.
(27) Moreno-Pineda, E.; Taran, G.; Wernsdorfer, W.; Ruben, M. Quantum Tunnelling of the Magnetisation in Single-Molecule Magnet Isotopologue Dimers. *Chem. Sci.* **2019**, *10* (19), 5138−5145.
(28) Tesi, L.; Salman, Z.; Cimatti, I.; Pointillart, F.; Bernot, K.; Mannini, M.; Sessoli, R. Isotope Effects on the Spin Dynamics of Single-Molecule Magnets Probed Using Muon Spin Spectroscopy. *Chem. Commun.* **2018**, *54* (56), 7826−7829.
(29) Pointillart, F.; Bernot, K.; Golhen, S.; le Guennic, B.; Guizouarn, T.; Ouahab, L.; Cador, O. Magnetic Memory in an Isotopically Enriched and Magnetically Isolated Mononuclear Dysprosium Complex. *Angew. Chem.* **2015**, *127* (5), 1524−1527.
(30) Huang, G.; Yi, X.; Jung, J.; Guillou, O.; Cador, O.; Pointillart, F.; le Guennic, B.; Bernot, K. Optimization of Magnetic Relaxation and Isotopic Enrichment in Dimeric DyIII Single-Molecule Magnets. *Eur. J. Inorg. Chem.* **2018**, *2018* (3), 326−332.
(31) Kishi, Y.; Pointillart, F.; Lefeuvre, B.; Riobé, F.; le Guennic, B.; Golhen, S.; Cador, O.; Maury, O.; Fujiwara, H.; Ouahab, L. Isotopically Enriched Polymorphs of Dysprosium Single Molecule Magnets. *Chem. Commun.* **2017**, *53* (25), 3575−3578.
(32) Biard, H.; Moreno-Pineda, E.; Ruben, M.; Bonet, E.; Wernsdorfer, W.; Balestro, F. Increasing the Hilbert Space Dimension Using a Single Coupled Molecular Spin. *Nat. Commun.* **2021**, *12* (1), No. 4443.
(33) Moreno-Pineda, E.; Klyatskaya, S.; Du, P.; Damjanović, M.; Taran, G.; Wernsdorfer, W.; Ruben, M. Observation of Cooperative Electronic Quantum Tunneling: Increasing Accessible Nuclear States in a Molecular Qudit. *Inorg. Chem.* **2018**, *57* (16), 9873−9879.
(34) Brietzke, T.; Mickler, W.; Kelling, A.; Holdt, H. J. Mono- and Dinuclear Ruthenium(II) 1,6,7,12-Tetraazaperylene Complexes. *Dalton Trans.* **2012**, *41* (9), 2788−2797.
(35) Brietzke, T.; Dietz, T.; Kelling, A.; Schilde, U.; Bois, J.; Kelm, H.; Reh, M.; Schmitz, M.; Körzdörfer, T.; Leimkühler, S.; Wollenberger, U.; Krüger, H. J.; Holdt, H. J. The 1,6,7,12-Tetraazaperylene Bridging Ligand as an Electron Reservoir and Its Disulfonato Derivative as Redox Mediator in an Enzyme−Electrode Process. *Chem. - Eur. J.* **2017**, *23* (62), 15583−15587.
(36) Goodwin, C. A. P.; Reta, D.; Ortu, F.; Chilton, N. F.; Mills, D. P. Synthesis and Electronic Structures of Heavy Lanthanide Metallocenium Cations. *J. Am. Chem. Soc.* **2017**, *139* (51), 18714−18724.
(37) Chen, Y. C.; Liu, J. L.; Wernsdorfer, W.; Liu, D.; Chibotaru, L. F.; Chen, X. M.; Tong, M. L. Hyperfine-Interaction-Driven Suppression of Quantum Tunneling at Zero Field in a Holmium(III) Single-Ion Magnet. *Angew. Chem., Int. Ed.* **2017**, *56* (18), 4996−5000.
(38) Dolai, M.; Moreno-Pineda, E.; Wernsdorfer, W.; Ali, M.; Ghosh, A. Exchange-Bias Quantum Tunneling of the Magnetization in a Dysprosium Dimer. *J. Phys. Chem. A* **2021**, *125*, 8230−8237.
(39) Pineda, E. M.; Lan, Y.; Fuhr, O.; Wernsdorfer, W.; Ruben, M. Exchange-Bias Quantum Tunnelling in a CO2-Based Dy4-Single Molecule Magnet. *Chem. Sci.* **2017**, *8* (2), 1178−1185.
(40) Wernsdorfer, W.; Aliaga-Alcalde, N.; Hendrickson, D. N.; Christou, G. Exchange-Biased Quantu Tunnelling in a Supramolecula Dimer of Single-Molecule Magnets. *Nature* **2002**, *416* (6879), 406−409.
(41) Bagai, R.; Wernsdorfer, W.; Abboud, K. A.; Christou, G. Exchange-Biased Dimers of Single-Molecule Magnets in OFF and ON States. *J. Am. Chem. Soc.* **2007**, *129* (43), 12918−12919.
(42) Han, T.; Giansiracusa, M. J.; Li, Z. H.; Ding, Y. S.; Chilton, N. F.; Winpenny, R. E. P.; Zheng, Y. Z. Exchange-Biasing in a Dinuclear Dysprosium(III) Single-Molecule Magnet with a Large Energy Barrier for Magnetisation Reversal. *Chem. - Eur. J.* **2020**, *26* (30), 6773−6777.
(43) Wernsdorfer, W. From Micro- to Nano-SQUIDs: Applications to Nanomagnetism. *Supercond. Sci. Technol.* **2009**, *22* (6), No. 064013.
(44) Wernsdorfer, W.; Chakov, N. E.; Christou, G. Determination of the Magnetic Anisotropy Axes of Single-Molecule Magnets. *Phys. Rev. B* **2004**, *70* (13), No. 132413.
(45) Lunghi, A.; Totti, F.; Sessoli, R.; Sanvito, S. The Role of Anharmonic Phonons in Under-Barrier Spin Relaxation of Single Molecule Magnets. *Nat. Commun.* **2017**, *8*, No. 14620.
(46) Lines, M. E. Orbital Angular Momentum in the Theory of Paramagnetic Clusters. *J. Chem. Phys.* **1971**, *55* (6), 2977−2984.
(47) Moreno Pineda, E.; Chilton, N. F.; Marx, R.; Dörfel, M.; Sells, D. O.; Neugebauer, P.; Jiang, S.-D.; Collison, D.; van Slageren, J.; McInnes, E. J. L.; Winpenny, R. E. P. Direct Measurement of Dysprosium(III)dysprosium(III) Interactions in a Single-Molecule Magnet. *Nat. Commun.* **2014**, *5* (1), No. 5243.
(48) Long, J.; Habib, F.; Lin, P. H.; Korobkov, I.; Enright, G.; Ungur, L.; Wernsdorfer, W.; Chibotaru, L. F.; Murugesu, M. Single-Molecule Magnet Behavior for an Antiferromagnetically Superexchange-Coupled Dinuclear Dysprosium(III) Complex. *J. Am. Chem. Soc.* **2011**, *133* (14), 5319−5328.
(49) Chilton, N. F.; Anderson, R. P.; Turner, L. D.; Soncini, A.; Murray, K. S. PHI: A Powerful New Program for the Analysis of Anisotropic Monomeric and Exchange-Coupled Polynuclear d- and f-Block Complexes. *J. Comput. Chem.* **2013**, *34* (13), 1164−1175.
(50) Jenkins, T. F.; Woen, D. H.; Mohanam, L. N.; Ziller, J. W.; Furche, F.; Evans, W. J. Tetramethylcyclopentadienyl Ligands Allow Isolation of Ln(II) Ions across the Lanthanide Series in [K(2.2.2-Cryptand)][(C5Me4H)3Ln] Complexes. *Organometallics* **2018**, *37* (21), 3863−3873.

(51) Huh, D. N.; Ziller, J. W.; Evans, W. J. Isolation of Reactive Ln(Ii) Complexes with C5H4Me Ligands (CpMe) Using Inverse Sandwich Countercations: Synthesis and Structure of [(18-Crown-6)K(μ-CpMe)K(18-Crown-6)][CpMe3LnII] (Ln = Tb, Ho). *Dalton Trans.* **2018**, *47* (48), 17285−17290.
(52) Gould, C. A.; McClain, K. R.; Yu, J. M.; Groshens, T. J.; Furche, F.; Harvey, B. G.; Long, J. R. Synthesis and Magnetism of Neutral, Linear Metallocene Complexes of Terbium(II) and Dysprosium(II). *J. Am. Chem. Soc.* **2019**, *141* (33), 12967−12973.
(53) Kundu, K.; White, J. R. K.; Moehring, S. A.; Yu, J. M.; Ziller, J. W.; Furche, F.; Evans, W. J.; Hill, S. A 9.2-GHz Clock Transition in a Lu(II) Molecular Spin Qubit Arising from a 3,467-MHz Hyperfine Interaction. *Nat. Chem.* **2022**, *14* (4), 392−397.
(54) Smith, R. L.; Wysocki, A. L.; Park, K. Electrically Tuned Hyperfine Spectrum in Neutral Tb(Ii)(CpiPr5)2single-Molecule Magnet. *Phys. Chem. Chem. Phys.* **2020**, *22* (38), 21793−21800.
(55) Shakurov', G. S.; Tarasov', V.; Malkin', B. Z.; Iskhakova, A.; Kasatkina3, L. A.; Heber', J.; Altwein, M. Hyperfine Structure of Submillimeter EPR Spectra of Non-Kramers Lanthanide Ions in Crystals. *Appl. Magn. Reson.* **1998**, *14*, 415−426, DOI: 10.1007/BF03161851.
(56) Wysocki, A. L.; Park, K. Hyperfine and Quadrupole Interactions for Dy Isotopes in DyPc2 Molecules. *J. Phys.: Condens. Matter* **2020**, *32* (27), No. 274002.
(57) Wysocki, A. L.; Park, K. Nature of Hyperfine Interactions in TbPc2 Single-Molecule Magnets: Multiconfigurational Ab Initio Study. *Inorg. Chem.* **2020**, *59* (5), 2771−2780.